Optics Letters

Selective excitation of four-wave mixing by helicity in gated graphene

Di Huang,[1] Tao Jiang,[1,2] Yangfan Yi,[1] Yuwei Shan,[1,3] Yingguo Li,[1] Zhihong Zhang,[4] Kaihui Liu,[4] Wei-Tao Liu,[1] and Shiwei Wu[1,5,6,7,*]

[1]State Key Laboratory of Surface Physics, Key Laboratory of Micro and Nano Photonic Structures (MOE), and Department of Physics, Fudan University, Shanghai 200433, China
[2]MOE Key Laboratory of Advanced Micro-Structured Materials, Shanghai Research Institute for Intelligent Autonomous Systems, and School of Physics Science and Engineering, Tongji University, Shanghai 200092, China
[3]Changchun Institute of Optics, Fine Mechanics and Physics, Chinese Academy of Sciences, Changchun 130033, China
[4]State Key Laboratory for Mesoscopic Physics, Frontiers Science Center for Nano-Optoelectronics, School of Physics, Peking University, Beijing, China
[5]Shanghai Qi Zhi Institute, Shanghai 200232, China
[6]Institute for Nanoelectronic Devices and Quantum Computing, Fudan University, Shanghai 200433, China
[7]Shanghai Research Center for Quantum Sciences, Shanghai 201315, China
*Corresponding author: swwu@fudan.edu.cn

Received 23 September 2021; revised 13 November 2021; accepted 22 November 2021; posted 23 November 2021; published 4 January 2022

Gapless Dirac fermions in monolayer graphene give rise to an abundance of peculiar physical properties, including exceptional broadband nonlinear optical responses. By tuning the chemical potential, stacking order, and photonic structures, the effective modulation of nonlinear optical phenomena in graphene has been demonstrated in recent years. Here, we demonstrate that optical helicity can be used as an extra tuning knob for four-wave mixing in gated graphene. Our results reveal the helicity selection rule for four-wave mixing in monolayer graphene, revealing nearly perfect circular polarization. Corresponding theoretical interpretations of the helicity selection rule that are also applicable to other nonlinear optical processes and materials are presented.

https://doi.org/10.1364/OL.443600

Introduction. Graphene, the first two-dimensional (2D) material to be discovered, has been investigated for over a decade [1,2]. The uniqueness of graphene mainly lies in its linear and gapless band structure at the corner of the hexagonal Brillouin zone (K point). In combination with other widely used tuning knobs for 2D materials, e.g., doping level, external field, strain, stacking orders, and twist angles, the massless Dirac fermions in graphene provide a platform with multiple degrees of freedom for the investigation of an abundance of physics, such as Klein tunneling in monolayer graphene and strong correlation physics in magic-angle twisted bilayer graphene.

The linear band structure in monolayer graphene induces strong optical nonlinearity, as first proposed in 2007 [3]. In brief, due to the constant Fermi velocity of carriers ($v_F \sim c/300$) at low energies, the "square-wave" optical current driven by a sinusoidal optical field naturally contains higher-order harmonic terms. While even-order nonlinear processes are forbidden in pristine monolayer graphene due to its inversion symmetry, various odd-order nonlinear optical processes, including third-harmonic generation (THG) [4–7], four-wave mixing (FWM) [6,8,9], self-phase modulation [10], saturable absorption [11], and high harmonic generation (HHG) [12], have been reported in recent years. Furthermore, modulations of the third-order nonlinear optical processes in graphene have been demonstrated by means of carrier doping [6,7], external photonic/plasmonic structures [13–15], stacking orders [16], and symmetry breaking [17]. It is noteworthy that the third-order nonlinear susceptibility was found to span several orders of magnitude upon varying the photon energy and doping level, and that the doping dependence of sum-frequency FWM contrasts sharply with that of difference-frequency FWM [6]. The synergy of these two aspects leaves plenty of room for the application of graphene nonlinear optics in regimes such as optoelectronics [18], all-optical signal processing [19], photonics, and optomechanics [20].

Although it is an essential tuning knob in optics, polarization is yet to be explored in graphene nonlinear optics. This is partially due to the isotropic response of third-harmonic generation, which shows the same polarization as the fundamental beam under linearly polarized excitation in normal incidence [4,6]. However, we cannot directly apply this perception to the circular polarization case, given that the underlying selection rule in nonlinear optics may be significantly modified during excitation with circularly polarized light [12,21,22]. In this paper, we report an investigation of the helicity selection of two-color FWM in ion-gel-gated monolayer graphene devices. The results showed that, when two beams that were circularly polarized with frequencies ω_1 and ω_2 and the same helicity were used along with monolayer graphene at a low doping level, only difference-frequency FWM signals at frequencies of $2\omega_1 - \omega_2$ and $2\omega_2 - \omega_1$ that had the same helicity as the excitation beams were observed. When the two excitation beams had opposite helicities and monolayer graphene with a high

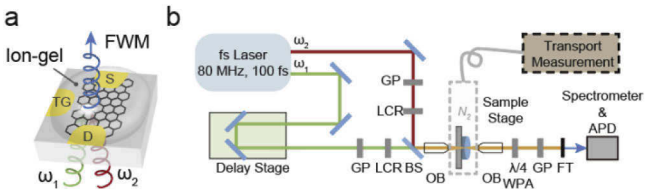

Fig. 1. Experimental setup. (a) Illustration of helicity-selective FWM in an ion-gel-gated graphene device. D: drain electrode, S: source electrode, TG: top gate electrode. (b) Illustration of the experimental setup for two-color four-wave mixing measurement. GP: Glan–Thompson polarizer, LCR: liquid-crystal retarder, BS: beam splitter, OB: objective, FT: filter, APD: avalanche photodiode. Ω_1 : 1.192 eV, ω_2 : 0.954 eV.

doping level was used, sum-frequency FWM signals at the frequencies $2\omega_1+\omega_2$ and $2\omega_2+\omega_1$ were solely observed, and the two branches showed a clear circular dichroism. Therefore, by combining optical helicity and electrical modulation, the selective excitation and pickup of a certain FWM branch was realized in graphene. We theoretically interpret the selection rule in graphene nonlinear optics with circularly polarized excitation light from the viewpoint of crystal symmetry and further discuss the selection rule for more general cases. Our results demonstrate that optical helicity is an important tuning knob for graphene nonlinear optics that has potential applications including, but not limited to, polarized light sources, polarized optical detection [23], all-optical signal processing [24], plasmonics [15], and the manipulation of spin state [25].

Methods. The experiment was done on ion-gel-gated graphene devices, as shown schematically in Fig. 1(a). The single-crystalline monolayer graphene was CVD grown by the method described in Ref. [26]. The devices were fabricated on fused silica substrate by the same protocol as reported in Ref. [6]. Source, drain, and top gate electrodes were patterned on graphene and substrate to form the graphene field-effect transistor. To maximize the tunability of the chemical potential of graphene while maintaining the optical transparency of the device, ion gel was chosen as the top gate dielectric material. The characterization of the chemical potential of graphene at a certain gate voltage was realized using transmittance spectra and ultrafast broadband photoluminescence, as described in Refs. [6,27]. Experimental measurements of the fabricated devices were conducted with a sample-scanning optical microscope at room temperature, a femtosecond laser system, and an electrical transport setup. During the experiment, the graphene device was protected by a dry nitrogen atmosphere to avoid humidity-induced degradation of device performance.

To realize the two-color FWM experiment, we used a dual-wavelength femtosecond laser system with a repetition rate of 80 MHz and a ~100 fs pulse duration (Insight Deepsee, Spectra Physics), which was capable of providing one tunable beam ranging from 680 nm (1.824 eV) to 1300 nm (0.954 eV) and another beam that was fixed at 1040 nm (1.192 eV). In our experiment, we chose photon energies of 1.192 eV (denoted the ω_1 beam) and 0.954 eV (denoted the ω_2 beam) to ensure that both the sum-frequency and difference-frequency FWM signals could be efficiently detected by our setup. A delay stage was placed in the light path of the ω_1 beam to find the time zero between the two beams. As shown in Fig. 1(b), a dedicated Glan–Thompson polarizer and a liquid-crystal retarder were used to generate nearly perfect circularly polarized light for each beam. The two beams were combined by a beam splitter and then sent collinearly into a sample-scanning optical microscope. To avoid any possible disturbance of the polarization by the beam splitter, we collected the signal in a transmission geometry. The polarization of the nonlinear optical signal was directly analyzed by a combination of a Fresnel-rhomb quarter-wave plate and a polarization analyzer followed by a liquid-nitrogen-cooled spectrometer.

Results and discussion. The helicity selection of two-color FWM in monolayer graphene was explored in four cases: both the ω_1 and ω_2 beams exhibited left-handed circular polarization (σ^+); both the ω_1 and ω_2 beams exhibited right-handed circular polarization (σ^-); the ω_1 beam exhibited σ^+ polarization and the ω_2 beam exhibited σ^- polarization; and the ω_1 beam exhibited σ^- polarization and the ω_2 beam exhibited σ^+ polarization. We started our investigation by focusing on difference-frequency FWM, which is known to have a larger third-order susceptibility at a low doping level [6]. When ω_1 and ω_2 had the same helicity, a two-color FWM signal centered at $2\omega_1-\omega_2$ with the same helicity as the excitation beams was observed, while the signal with the opposite helicity was negligible, as illustrated in Figs. 2(a) and 2(b). On the other hand, when the ω_1 and ω_2 beams had opposite helicities, no obvious difference-frequency

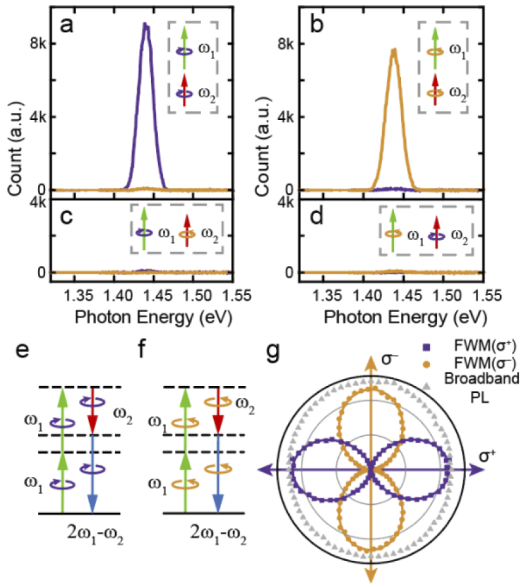

Fig. 2. Difference-frequency FWM signal in graphene with circularly polarized excitation light. (a)–(d) Difference-frequency FWM signal excited with 1040 nm (ω_1,1.192 eV) and 1300 nm (ω_2, 0.954 eV) input beams in various polarization configurations [(a), (b) both the ω_1 and ω_2 beams exhibit σ^+ (σ^-) polarization; (c) the ω_1 beam exhibits σ^+ polarization, and the ω_2 beam exhibits σ^- polarization; (d) the ω_1 beam exhibits σ^- polarization and the ω_2 beam exhibits σ^+ polarization]. The purple/dark gray (orange/light gray) lines indicate the analyzed signal with σ^+ (σ^-) polarization. Background ultrafast broadband photoluminescence was subtracted from all the spectra presented in (a)–(d). (e), (f) Energy diagrams illustrating the optical transitions of the difference-frequency FWM signals in (a) and (b), respectively. (g) Polarization patterns of the FWM signals in (a) and (b) (squares and circles, respectively) and the broadband ultrafast PL (triangles) after passing through a quarter-wave plate. The horizontal/vertical axis in the pattern indicates σ^+/σ^- polarization.

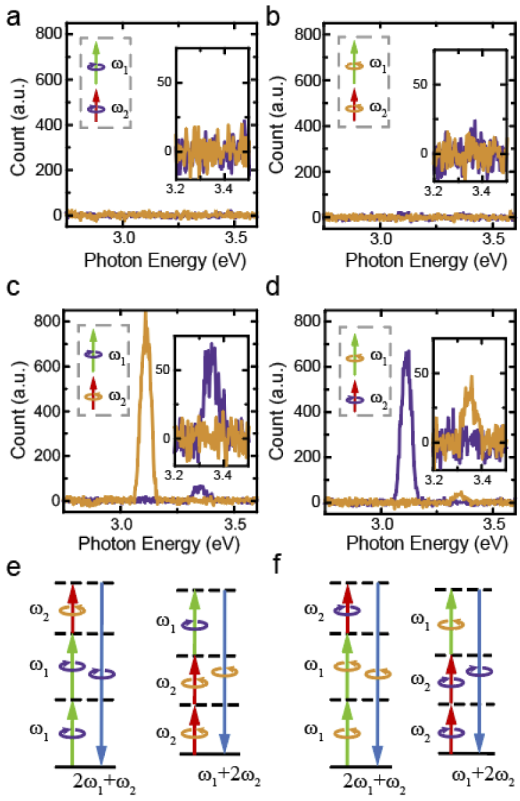

Fig. 3. Sum-frequency FWM signal in graphene with circularly polarized excitation light. (a)–(d) Sum-frequency FWM signal excited with 1040 nm (ω_1, 1.192 eV) and 1300 nm (ω_2, 0.954 eV) beams in various polarization configurations [(a), (b) both the ω_1 and ω_2 beams exhibit σ^+ (σ^-) polarization; (c) the ω_1 beam exhibits σ^+ polarization and the ω_2 beam exhibits σ^- polarization; (d) the ω_1 beam exhibits σ^- polarization and the ω_2 beam exhibits σ^+ polarization]. As in Fig. 2, the purple/dark gray (orange/light gray) lines indicate the analyzed signal with σ^+ (σ^-) polarization. Inset: Zoom of the 3.346 eV ($2\omega_1+\omega_2$) sum-frequency FWM signal. The sum-frequency FWM signal was taken with a graphene chemical potential $|2\mu| = 1.6$ eV to block one-photon resonance, which greatly enhances the sum-frequency FWM signal. (e), (f) Energy diagrams illustrating the generation of the sum-frequency FWM signals $2\omega_1+\omega_2$ and $\omega_1+2\omega_2$ in (c) and (d), respectively.

FWM was observed [Figs. 2(c) and 2(d)]. The optical transitions that occur with circularly polarized photons to generate the difference-frequency FWM signals are summarized in the energy diagrams shown in Figs. 2(e) and 2(f). Calculation of the degree of circular polarization $\rho = |I(\sigma^-)–I(\sigma^+)|/[I(\sigma^-)+I(\sigma^+)]$, in which $I(\sigma^+)/I(\sigma^-)$ stands for the intensity of the FWM signal with σ^+/σ^- helicity, respectively, showed that ρ is higher than 0.95 in our experiment, which contrasts sharply with depolarized broadband ultrafast photoluminescence (PL), as depicted in Fig. 2(g) [27]. In our experiment, only the upconversion branch at 1.434 eV (i.e., $2\omega_1-\omega_2$) involving two 1.192 eV photons and one 0.954 eV photon was observed; the downconversion branch at 0.716 eV involving two 0.954 eV photons and one 1.192 eV photon (i.e., $2\omega_2-\omega_1$) was not observed due to the limited spectral range of our silicon detector. However, considering that the downconversion branch is the counterpart of the upconversion branch and is obtained by simply permuting the 1.192 eV and 0.954 eV photons in optical transitions, the downconversion branch is expected to follow the same helicity selection rule as the upconversion branch.

Table 1. Helicity Selection Rule for Two-Color FWM[a]

	σ^-/σ^-	σ^-/σ^+	σ^+/σ^-	σ^+/σ^+
$3\omega_1$	–	–	–	–
$2\omega_1+\omega_2$	–	σ^-	σ^+	–
$\omega_1+2\omega_2$	–	σ^+	σ^-	–
$3\omega_2$	–	–	–	–
$2\omega_1-\omega_2$	σ^-	–	–	σ^+
$2\omega_2-\omega_1$	σ^-	–	–	σ^+

[a]Helicities of excitation beams ω_1/ω_2 are shown in the table header. Dashes (–) in the table indicate forbidden nonlinear optical processes.

We then turned to study the sum-frequency two-color FWM signals. In the case of linear polarization, four signal branches centered at $3\omega_1$ (THG), $2\omega_1+\omega_2$, $\omega_1+2\omega_2$, and $3\omega_2$ (THG) are expected [6]. Due to the intrinsically low susceptibility of sum-frequency FWM in pristine graphene, we enhanced the FWM signals by tuning the chemical potential μ of the monolayer graphene to $2|\mu| \sim 1.6$ eV, which simultaneously suppressed the difference-frequency FWM [6]. When both the ω_1 and ω_2 beams had the same helicity σ^+ or σ^-, no obvious sum-frequency FWM signal was observed, as shown in Figs. 3(a) and 3(b), in contrast to the difference-frequency FWM signal discussed above. Intriguingly, when the ω_1 and ω_2 beams had opposite helicities, as shown in Figs. 3(c) and 3(d), sum-frequency FWM signals were observed, but THG signals were still missing. By comparing Figs. 3(c) and 3(d), we found that the high-energy branch at 3.346 eV ($2\omega_1+\omega_2$) showed the same helicity as the ω_1 beam while the low-energy branch at 3.107 eV ($\omega_1+2\omega_2$) showed the same helicity as the ω_2 beam. Similar to the difference-frequency case, the ρ of the sum-frequency FWM signal was greater than 0.95. Moreover, there was no THG signal in any of the excitation cases. The helicity-allowed optical transitions for sum-frequency two-color FWM are depicted in the energy diagrams of Figs. 3(e) and 3(f). To facilitate understanding, we summarize the helicity selection rule for two-color FWM in Table 1.

We used two different theoretical approaches to interpret the helicity selection rule for two-color FWM we described above. Briefly, from the viewpoint of crystalline structure, monolayer graphene belongs to centrosymmetric point group D_{6h}, which has one C_6 axis passing through the centrosymmetric point and perpendicular to the crystalline plane and six C_2 axes lying in the crystalline plane. Assuming that the graphene lies in the xy plane, if we consider a normally incident photon with respect to the crystalline plane, all the nonzero tensor elements of the third-order susceptibility ($\chi^{(3)}$) of graphene are

$$\chi^{(3)}_{xxxx} = \chi^{(3)}_{yyyy} = \chi^{(3)}_{xxyy} + \chi^{(3)}_{xyyx} + \chi^{(3)}_{xyxy},$$
$$\text{with} \begin{cases} \chi^{(3)}_{xxyy} = \chi^{(3)}_{yyxx} \\ \chi^{(3)}_{xyyx} = \chi^{(3)}_{yxxy} \\ \chi^{(3)}_{xyxy} = \chi^{(3)}_{yxyx} \end{cases}.$$

Given the isotropy of $\chi^{(3)}$ in graphene [6,28,29], we can set the in-plane coordinates to be in any direction and obtain the same result. A calculation based on these nonvanishing tensor elements reproduced the experimentally observed helicity selection rule for two-color FWM well. For more details about the calculation, please refer to Section 1 of Supplement 1.

Our results can be interpreted from the straightforward perspective of photon spin angular momentum conservation during the FWM process. The spin angular momentum carried by a single photon is $\hbar$ (for σ^+) or $-\hbar$ (for σ^-) along the axis of propagation [30]. Due to the degenerate valley, the absence of excitonic effects in the linear dispersion regime, and the six-fold rotational symmetry of graphene, the conservation of the out-of-plane angular momentum should follow $m\hbar = 6N\hbar \pm \hbar$ (m, N are integers) [31–33], where $m\hbar$ is the total spin angular momentum of the fundamental photons and $6N\hbar$ is the angular momentum provided by the crystal lattice [22]. For a third-order nonlinear optical process, the possible values of $m\hbar$ are $\pm 3\hbar$ when the three fundamental photons contribute the same spin angular momentum, or $\pm\hbar$ when one photon contributes the opposite angular momentum to the other two. The conservation of angular momentum can be fulfilled only when $N = 0$ and $m\hbar = \pm\hbar$ ($N = 0$ indicates that the total angular momentum transferred to the graphene lattice is zero). Therefore, the conservation of photon spin angular momentum in third-order nonlinear processes in graphene leads to an absence of third-harmonic generation signal in this case, and the helicity selection rule in two-color FWM. This photon spin angular momentum conservation was also derived in a general and strict way starting from the viewpoint of crystal symmetry and group theory, as discussed in Section 2 of Supplement 1. Following a similar derivation, we predicted the helicity selection rules for more general nonlinear optical processes, such as three-color FWM, as shown in Section 4 and Table S1 of Supplement 1.

Conclusion. In summary, we have presented and then theoretically explained the helicity-selective FWM signal in gated graphene. When exciting with different combinations of helicity, the selective excitation and circular dichroism of FWM signal was realized with the help of electrical doping, which shows $\rho \geq 0.95$ even at room temperature. Subsequent theoretical analysis of the experimental data further unveiled the working principle for controlling graphene FWM using helicity. Our results provide an ideal platform to realize graphene-based polarization-controlled nonlinear optical devices such as frequency converters [34] and shed light on the control of higher-order nonlinear optical processes. The theoretical derivations of the selection rule could easily be adapted to a broader range of nonlinear processes and materials.

Funding. National Key Research and Development Program of China (2019YFA0308404); National Natural Science Foundation of China (11991062, 12034003, 62005198, 91950201); Science and Technology Commission of Shanghai Municipality (2019SHZDZX01, 20JC1415900, 21JC1402000); Program of Shanghai Academic Research Leader (20XD1400300); Shanghai Municipal Education Commission (2021KJKC-03-61); Shanghai Pujiang Talent Plan (20PJ1414100).

Disclosures. The authors declare no conflicts of interest.

Data availability. Data underlying the results presented in this paper are not publicly available at this time but may be obtained from the authors upon reasonable request.

Supplemental document. See Supplement 1 for supporting content.

REFERENCES

1. K. S. Novoselov, A. K. Geim, S. V. Morozov, D. Jiang, Y. Zhang, S. V. Dubonos, I. V. Grigorieva, and A. A. Firsov, Science **306**, 666 (2004).
2. K. S. Novoselov, V. I. Fal'ko, L. Colombo, P. R. Gellert, M. G. Schwab, and K. Kim, Nature **490**, 192 (2012).
3. S. A. Mikhailov, Europhys. Lett. **79**, 27002 (2007).
4. S.-Y. Hong, J. I. Dadap, N. Petrone, P.-C. Yeh, J. Hone, and R. M. Osgood, Phys. Rev. X **3**, 021014 (2013).
5. N. Kumar, J. Kumar, C. Gerstenkorn, R. Wang, H.-Y. Chiu, A. L. Smirl, and H. Zhao, Phys. Rev. B **87**, 121406 (2013).
6. T. Jiang, D. Huang, J. Cheng, X. Fan, Z. Zhang, Y. Shan, Y. Yi, Y. Dai, L. Shi, K. Liu, C. Zeng, J. Zi, J. E. Sipe, Y.-R. Shen, W.-T. Liu, and S. Wu, Nat. Photonics **12**, 430 (2018).
7. G. Soavi, G. Wang, H. Rostami, D. G. Purdie, D. De Fazio, T. Ma, B. Luo, J. Wang, A. K. Ott, D. Yoon, S. A. Bourelle, J. E. Muench, I. Goykhman, S. Dal Conte, M. Celebrano, A. Tomadin, M. Polini, G. Cerullo, and A. C. Ferrari, Nat. Nanotechnol. **13**, 583 (2018).
8. E. Hendry, P. J. Hale, J. Moger, A. K. Savchenko, and S. A. Mikhailov, Phys. Rev. Lett. **105**, 097401 (2010).
9. S. Shareef, Y. S. Ang, and C. Zhang, J. Opt. Soc. Am. B **29**, 274 (2012).
10. R. Wu, Y. Zhang, S. Yan, F. Bian, W. Wang, X. Bai, X. Lu, J. Zhao, and E. Wang, Nano Lett. **11**, 5159 (2011).
11. Z. Sun, T. Hasan, F. Torrisi, D. Popa, G. Privitera, F. Wang, F. Bonaccorso, D. M. Basko, and A. C. Ferrari, ACS Nano **4**, 803 (2010).
12. N. Yoshikawa, T. Tamaya, and K. Tanaka, Science **356**, 736 (2017).
13. H. Zhou, T. Gu, J. F. McMillan, N. Petrone, A. Van Der Zande, J. C. Hone, M. Yu, G. Lo, D.-L. Kwong, G. Feng, S. Zhou, and C. W. Wong, Appl. Phys. Lett. **105**, 091111 (2014).
14. J. D. Cox and F. Javier García De Abajo, Nat. Commun. **5**, 5725 (2014).
15. T.-T. Kim, S. S. Oh, H.-D. Kim, H. S. Park, O. Hess, B. Min, and S. Zhang, Sci. Adv. **3**, e1701377 (2017).
16. Y. Shan, Y. Li, D. Huang, Q. Tong, W. Yao, W. T. Liu, and S. Wu, Sci. Adv. **4**, eaat0074 (2018).
17. Y. Zhang, D. Huang, Y. Shan, T. Jiang, Z. Zhang, K. Liu, L. Shi, J. Cheng, J. E. Sipe, W. T. Liu, and S. Wu, Phys. Rev. Lett. **122**, 047401 (2019).
18. T. Gu, N. Petrone, J. F. McMillan, A. van der Zande, M. Yu, G. Q. Lo, D. L. Kwong, J. Hone, and C. W. Wong, Nat. Photonics **6**, 554 (2012).
19. M. Romagnoli, V. Sorianello, M. Midrio, F. H. L. Koppens, C. Huyghebaert, D. Neumaier, P. Galli, W. Templ, A. D'Errico, and A. C. Ferrari, Nat. Rev. Mater. **3**, 392 (2018).
20. Y. Tian, H. Tian, Y. L. Wu, L. L. Zhu, L. Q. Tao, W. Zhang, Y. Shu, D. Xie, Y. Yang, Z. Y. Wei, X. H. Lu, T.-L. Ren, C.-K. Shih, and J. Zhao, Sci. Rep. **5**, 10582 (2015).
21. J. Cheng, D. Huang, T. Jiang, Y. Shan, Y. Li, S. Wu, and W. T. Liu, Opt. Lett. **44**, 2141 (2019).
22. J. Xiao, Z. Ye, Y. Wang, H. Zhu, Y. Wang, and X. Zhang, Light: Sci. Appl. **4**, e366 (2015).
23. R. Farshchi, M. Ramsteiner, J. Herfort, A. Tahraoui, and H. T. Grahn, Appl. Phys. Lett. **98**, 162508 (2011).
24. A. E. Willner, S. Khaleghi, M. R. Chitgarha, and O. F. Yilmaz, J. Lightwave Technol. **32**, 660 (2014).
25. E. Togan, Y. Chu, A. S. Trifonov, L. Jiang, J. Maze, L. Childress, M. V. G. Dutt, A. S. Sørensen, P. R. Hemmer, A. S. Zibrov, and M. D. Lukin, Nature **466**, 730 (2010).
26. X. Xu, Z. Zhang, L. Qiu, J. Zhuang, L. Zhang, H. Wang, C. Liao, H. Song, R. Qiao, P. Gao, Z. Hu, L. Liao, Z. Liao, D. Yu, E. Wang, F. Ding, H. Peng, and K. Liu, Nat. Nanotechnol. **11**, 930 (2016).
27. D. Huang, T. Jiang, Y. Zhang, Y. Shan, X. Fan, Z. Zhang, Y. Dai, L. Shi, K. Liu, C. Zeng, J. Zi, W. T. Liu, and S. Wu, Nano Lett. **18**, 7985 (2018).
28. R. W. Boyd, *Nonlinear Optics* (Academic, 2008).
29. Y.-R. Shen, *The Principles of Nonlinear Optics* (Wiley-Interscience, 1984).
30. R. A. Beth, Phys. Rev. **50**, 115 (1936).
31. H. J. Simon and N. Bloembergen, Phys. Rev. **171**, 1104 (1968).
32. N. Bloembergen, J. Opt. Soc. Am. **70**, 1429 (1980).
33. S. Chen, G. Li, F. Zeuner, W. H. Wong, E. Y. B. Pun, T. Zentgraf, K. W. Cheah, and S. Zhang, Phys. Rev. Lett. **113**, 033901 (2014).
34. N. Vermeulen, J. Cheng, J. E. Sipe, and H. Thienpont, IEEE J. Sel. Top. Quantum Electron. **22**, 347 (2016).